HYDROBORATION REACTION: THE EFFECT OF B AND N ATOMS DOPING ONTO THE (5,5) ARMCHAIR SIDEWALLS OF SINGLE-WALL CARBON NANOTUBES (SWNTs)

INTRODUCTION

Carbon nanotubes, especially single-walled carbon nanotubes (SWNTs) have become one of the most potentially versatile nanoscale materials since their discovery by Iijima *et al.* in 1991. CNTs exhibit exceptional electronic, mechanical, thermal, and transport properties for universal use in ultra small nano-electronic, -mechanical, -electromechanical, -chemical, -composites and scanning probe devices. Carbon nanotubes have been regarded as materials (Ebbesen et al., 1992) most naturally related to the other intractable carbon allotropes - graphite, diamond, and fullerene-like structures (Kroto *et al.*, 1985). Carbon nanotubes consist of a shell of sp2-hybridized carbon atoms forming a hexagonal network similar to a graphene sheet, which has been rolled up into a cylindrical shape. There are two main types of carbon nanotubes. Multiwalled nanotubes (MWNTs) (Iijima *et al.*, 1991) comprise an array of such nanotubes that are concentrically nested like the rings of a tree trunk (Fig. 1) with outer diameters of 3–30 nm and lengths of up to 1 μm. Single-walled carbon nanotubes (SWCNT) (Bethune *et al.* and Iijima *et al.*, 1993) are composed of a single graphene sheet rolled into a seamless cylindrical structure with diameters ranging from 0.4 to 2–3 nm and lengths usually of microscopic order (Fig. 2).

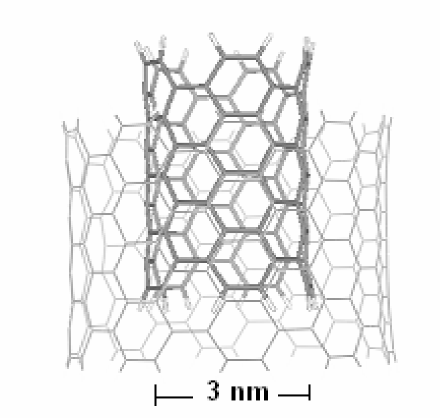

Figure 1 Multi-walled carbon nanotubes discovered in 1991.

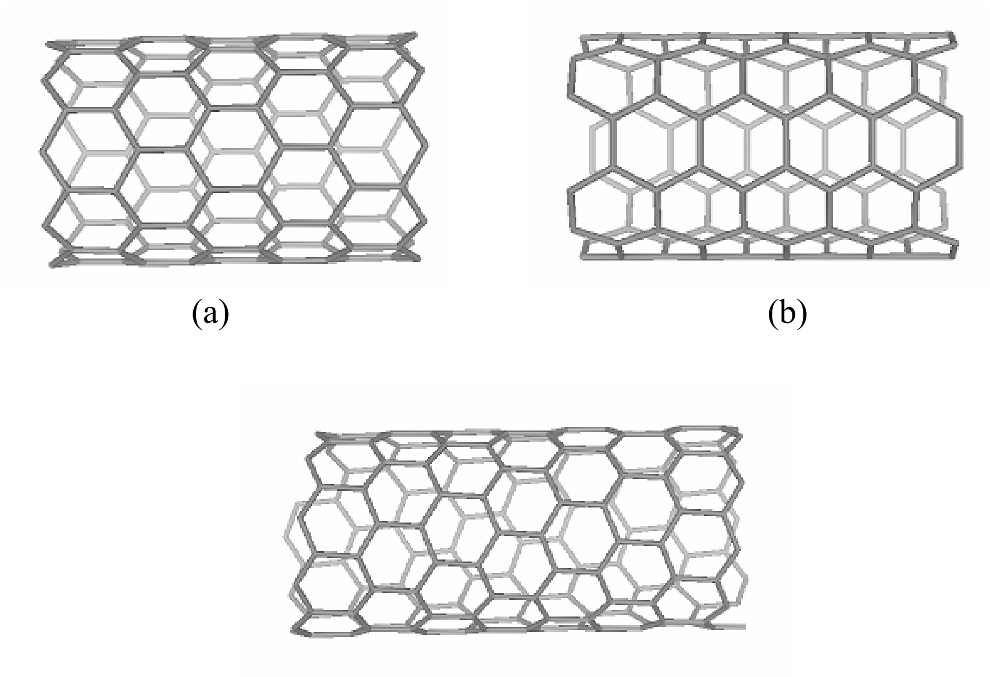

Figure 2 (a) Zigzag [9,0] nanotube. (b) armchair [5,5] nanotube. (c) chiral [9,1] nanotube. The numbers in parentheses are the chiral indices.

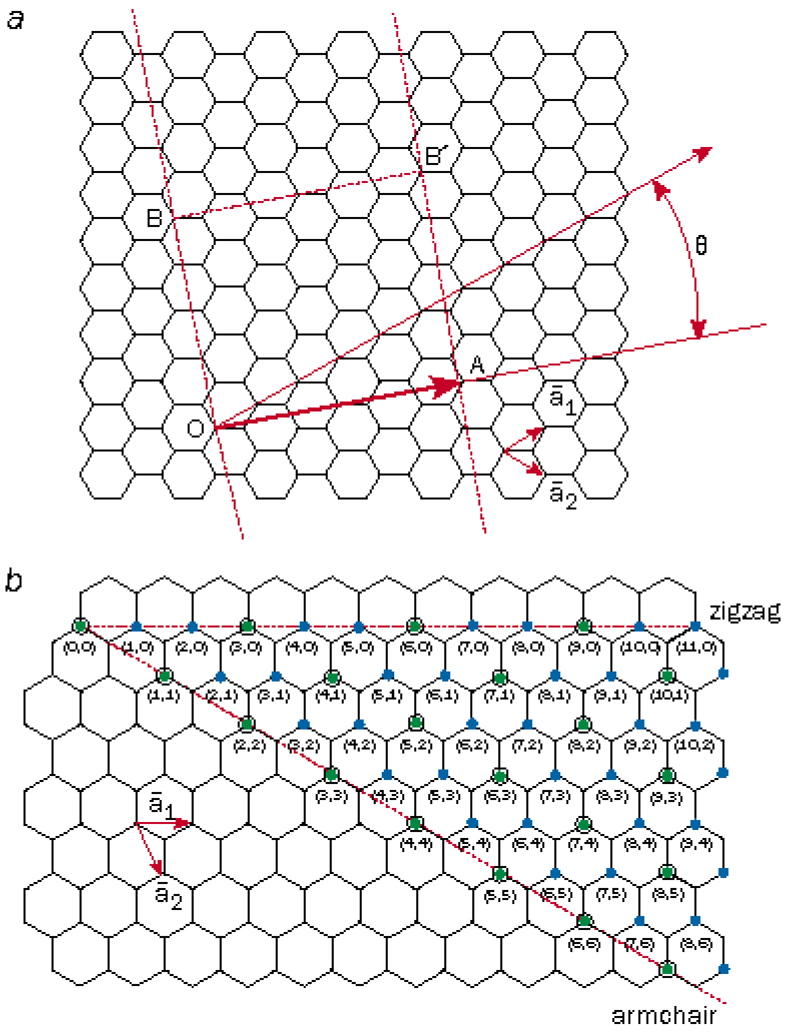

Figure 3 Flat hexagon lattices of a graphene sheet.

Despite structural similarity to a single sheet of graphite, which is a semiconductor with a zero band gap, SWNTs may be either metallic or semiconducting, depending on the sheet direction. SWNTs are defined by a chiral vector; C_h, defined as $n\mathbf{a}_1 + m\mathbf{a}_2$, which connects two crystallographically equivalent sites on a graphene sheet (where $\mathbf{a}_1$ and $\mathbf{a}_2$ are unit vectors of the hexagonal honeycomb lattice and n and m are integers) (see Figure 3). This chiral vector $\mathbf{C}_h$ also defines a chiral angle; θ, which is the angle between $\mathbf{C}_h$ and the zigzag direction of the graphene sheet (Figure 3). Each nanotube‘s topology is usually characterized by these two integer numbers (n,m), thus defining some peculiar symmetries such as *armchair* (n,n) and *zigzag* $(n,0)$ or chiral (any other *n* and *m*) classes. The electronic properties of nanotubes vary in a periodic way between being metallic and semiconductor and follow a general rule: all armchair SWNTs are metals; those with $n - m = 3k$, where k is a nonzero integer, are semiconductors with a tiny band gap; and all others are semiconductors with a band gap that inversely depends on the nanotubes diameter (Saito *et al.,* 1992)

The unique structure-dependent properties of SWNTs have intrigued researchers of one-dimensional fields for various applications. SWNTs have also unique, and in many ways extraordinary, mechanical strength, greater than that of Fe, they have high resilience, density lower than that of Al, thermal stability at 1400°C in a vacuum, and high current carrying capacity. The structure of bundles of SWNTs closely mimics that of a porous material with nanometer spaces available both inside the tubes and also in the interstitial spaces between them. The spaces are available for the storage of adsorbed gases, particularly hydrogen adsorption as shown in a recent report(Dillon et al.) that stated 10-wt% hydrogen uptake by SWNTs is possible. These can be a widely applied application for fuel-cell development and a source of clean energy. SWNTs can emit electrons from their tip by the local field source, can be used practically as field emission electron sources for flat panel displays (Lee *et al.*, 2001). Additionally, they have low power consumption, high brightness, and a long lifetime, comparable to liquid crystal displays. Another intriguing possibility is that we can use the hollow space inside SWNTs, such C60 molecules, known as peapods, discovered by Iijima *et al.*, 2002 These objects provide interesting probabilities in physics, chemistry, and perhaps in the future, biology.

The structural component of SWNTs was divided into two different curvature regions: the sidewall and the capped end. Carbon nanotubes can be capped at each end (Dresselhaus et al., 1995) by bisecting a C60 molecule at the equator and joining the two resulting hemispheres with a cylindrical tube of the same diameter as the C60 molecule (Wang *et al.,* 2000; Tang *et al.,* 2001; Saito *et al.,* 1992). If the molecule is bisected normally to a 5-fold axis, the capped armchair tube (Fig. 4a) is obtained. On the other hand, if the molecule is bisected normally to a 3-fold axis, the capped zigzag tube (Fig. 4b) is generated. Fig. 4c shows a general capped chiral tube. Nanotubes of larger diameter can be capped with larger fullerene molecules, such as C70 and C80 molecules.

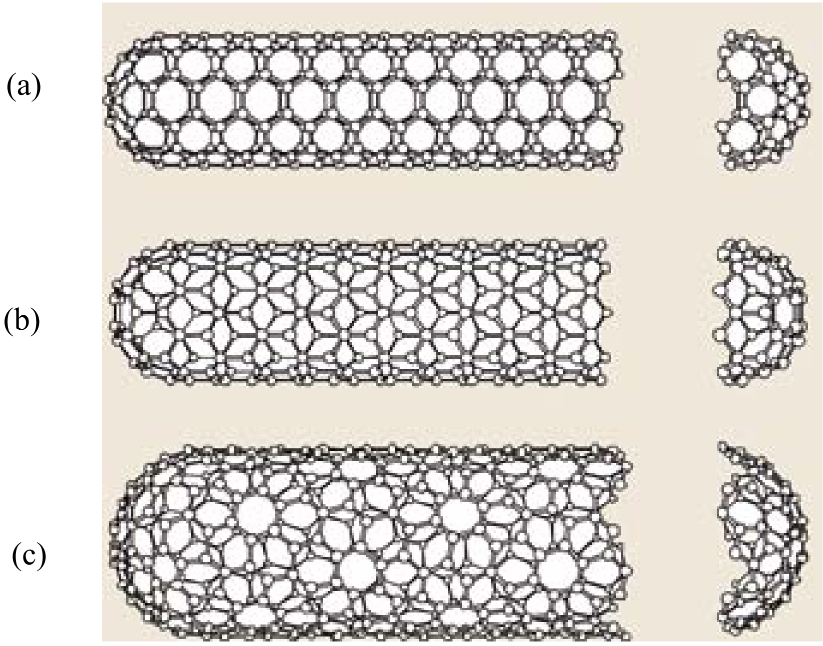

Figure 4 Models of capped SWCNTs, showing: (a) the armchair, (n,n), tube; (b) the zigzag, (n,0), tube; (c) the chiral (2n,n), tube.

The perfect SWNTs have a quite high chemical stability; however, they are expected to be more reactive than the flat graphene sheet with the curvature of the tube. From the viewpoint of chemistry, curvature-induced pyramidalization (θ_p), and misalignment of the π-orbitals of the carbon atoms induce a local strain, and the chemical reactivity of carbon nanotubes is driven by an enormous strain from their spherical geometry by accelerating the strain relief to strongly favor additional chemistry (Haddon *et al.*, 1993 and Hirsch *et al.*, 2002). Consequently, the capped end will always be more reactive than the sidewalls. For example, in the (5,5) SWNT shown in Figure 4a, which is capped by a hemisphere of C60, the pyramidalization angles are as follow: $\theta_p = 11.6°$ (end cap) and $\theta_p = 6.0°$ (sidewall) (Hamon *et al.*).

Although SWNTs represent a powerful substance in emerging areas on nanotubes-based materials, it seems hard to say that the real opportunities for SWNT's chemistry still lie in the future because SWNTs exhibit insolubility which is challenging for separation or purification, and utilization for applications. In order to remove the limitations of the uses of SWNTs, chemical functionalization of SWNTs, especially the covalent sidewalls functionalization (Niyoki *et al.,* 2002; Sun *et al.*, 2002; Stanislaus *et al.*, 1998) is regarded. The functionalized sidewalls of SWNTs have been widely practical used since the high degree of chemical functionalization possible through covalent sidewalls for their solubilization (Hirsch *et al.*, 2002; Sinnott *et al.*, 2002; Bahr *et al.*, 2002). Recently, covalent chemical functionalization of the sidewalls of single-wall carbon nanotubes (SWNTs) has been demonstrated in both experimental and theoretical studies via the fluorine addition (Cioslowski *et al.,* 2002), the ozonization (Lu *et al.,* 2002), the Diels-Alder reaction (Lu *et al.,* 2002), the oxycarbonyl nitrene cycloaddition (Holzinger *et al.,* 2003), the Bingel reaction (Coleman *et al.,* 2003), the dichlorocarbene addition (Hu *et al.,* 2003), 1,3-dipolar cycloadditions (Lu *et al.,* 2003), the retro-cycloaddition reaction (Martin *et al.,* 2006), the dipyridyl imidazolidene (Kang *et al.,* 2004), the addition of 2-carboxyethyl or 3-carboxypropyl addition (Peng *et al.,* 2003), and the hydroboration reaction (Long *et al.,* 2003).

From previous studies, organoborane products, readily available via the hydroboration of unsaturated organic compounds, exhibit a remarkable versatility in mild condition (Brown *et al.*, 1956). The hydroboration reaction is asymmetric synthesis, and Anti-Markownikoff hydration of olefins, both high regioselectivity and stereoselectivity. With the double character of ethylene structure, it similar to Moreover, the hydroboration of fullerenes have been successfully carried out in experimental studies in which it was found that the hydroboration reaction of C60 and C70 is facile and yielded toward specific sites at [6,6] fused-membered ring by regiochemistry. The reaction demonstrated that it has not only high site selectivity but also is rapidly further functionalized by easily occurring hydrogenated products (Cahill and Henderson *et al.*, 1996). Later, Toganoh *et al.*, 2003 reported that the synthesis of rhodium complexes bearing the (PhCH2)2PhC60 ligand was successful via the hydroboration reaction and synthesized regioselective fullerene tri-adducts in 93-96% yields. A recent theoretical study (Lu *et al.*, 2003) proved the hydroboration reaction of fullerene by using the ONIOM (B3LYP/6-31G*:AM1) method, which could occur readily, obtained the reaction energy of -15.1 kcal/mol, which considered with full geometry optimizations performed at the B3LYP/6-31G* level predicted that the reaction energy is -15.0 kcal/mol. The hydroboration of the sidewalls of *(5,5)* armchair SWNTs was investigated at the same level of theory and was found to be thermoneutral (Lu *et al.*, 2003).

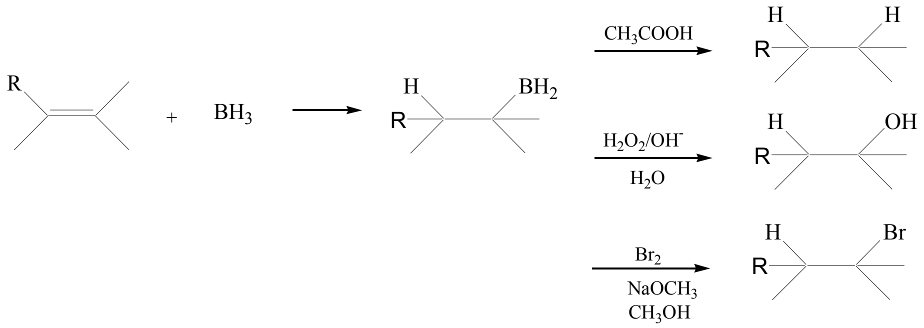

Figure 5 The hydroboration reaction of ethylene with borane (BH_3) and then further functionalized to alkane, alcohol, and alkyl bromide under mild conditions.

Soon after the discovery of carbon nanotubes by Ijima in 1991, B and N atoms doped into SWNTs became a state-of-the-art direction in nanotube science, and they have also been synthesized by a carbon nanotubes substitution reaction in which carbon atoms of starting CNTs are substituted partially or totally by boron and/or nitrogen atoms by reaction with B_2O_3 under Ar or N_2 atmosphere (Han *et al.*, 2001). Both boron- and nitrogen-doped tubes are metallic with no apparent band gap, in contrast to undoped tubes with varying electronic character, it is anticipated that the BN-doped nanotubes will have many novel electronic, mechanical, conductive and optical properties. Thus, they possess potential for applications in many fields, such as nanosized photonic (Wang *et al.*, 2003) and electronic (Mickelson *et al.*,2003) devices, electron field emitters (Charlier *et al.*, 2002), sensitive sensors (Shu *et al.*, 2003). The B–N ring doped of (5,0) and (5,5) armchair single-wall carbon nanotubes investigated by semiempirical and B3LYP/STO-3G calculations suggested that the HOMO-LUMO gap became lower, comparable to undoped tubes and may be obtained exothermically from carbon nanotubes. Among these findings, the most intriguing one is perhaps the hybrid BN-doped SWNTs with equal-numbered B and N atoms because of their structural similarities and isoelectronic relationship with their parent carbon molecules. These have been investigated recently by several groups for their interesting electrochemistry properties, for example, Quinonero *et al.* have carried out theoretical investigations on boron and nitrogen-doped zigzag single-walled carbon nanotubes to explore their capability to incorporate Li+ ion in its interior, and found that the BN-doped nanotubes have higher interaction energies with lithium cation than the pure nanotubes (David *et al.*, 2005). Zhou *et al.* have investigated the lithium adsorption properties in nitrogen-doped and boron-doped nanotubes through first-principle calculations concluding that a boron-doped nanotube decreases the Li-adsorption energies and, on the contrary, a nitrogen-doped nanotube increases the Li-adsorption energies (Zhou *et al.*, 2004).

In this study, The hydroborations of the sidewalls of 5,5-armchair SWNTs and the BN doped (5,5) SWNTs have been investigates. The aims of this theoretical study using the ONIOM method are to: (i) determine the reaction mechanism of the hydroboration with borane onto the sidewalls of (5,5)-armchair SWNTs, (ii) examine the effects of the substitution of boron and nitrogen atoms onto the sidewalls of (5,5)-armchair SWNTs in the hydroboration reaction (iii) study the preference of the carbon reactive site for the attachment of borane to the sidewall of the BN doped (5,5) SWNT.

LITERATURE REVIEWS

Sumio Iijima *et al*., (1991) discovered microtubules of graphitic carbon, defined carbon nanotubes (CNT) with outer diameters of 4–30 nm and a length of up to 1 mm, by an arc-discharge of graphite. These tubules consisted of two or more seamless graphene cylinders concentrically arranged. The innermost tubes of the tubules had diameters as small as 2.2 nm in some of the observations. Electron diffraction analysis showed that the crystal axis of the graphene sheets in some of the tubes had a helical arrangement relative to the tube axis. These tubes were called multi-wall carbon nanotubes (MWNT). The unique properties of these structures promised unimaginable applicability and thus attracted a great deal of interest that continues to this day. For example, super high quality MWNTs have recently been produced by carbon evaporation using a high-frequency plasma, Koshio *et al*. Later, Bethune *et al*., (1993) and Iijima *et al*., (1993) first reported single-wall carbon nanotubes (SWNT), which are seamless cylinders, each made of a single graphene sheet possessing diameters ranging from 0.4 to 2–3 nm, and their length in the micrometer order. SWNTs usually come together to form bundles. In a bundle, the SWNTs are hexagonally arranged to form a crystal-like structure, Smalley *et al*. The electronic properties of SWNTs were found to depend on their atomic structures, described by their chiral angle and diameter, which are specified by the lattice indices [n,m] (Saito *et al.,* 1992; Wildoer *et al.,* 1998). Atomically resolved scanning tunneling microscope (STM) images have subsequently been used to experimentally probe the structures of SWNTs and are also interpreted using these lattice indices (Odom *et al.,* 1998; Venerma *et al.,* 2000).

Chemical functionalization of SWNTs have been focused on by several research groups with the attachment of relatively large functional groups to tubes. In the first category of chemical functionalization, Margrave, Smalley, *et* *al.*, 1998 reported the fluorination of SWNTs by Raman studies at temperatures ranging from 150-325°C suggesting sidewall derivatization and fluorine added more favorably around the circumference of the tube, backed up by AM1 calculations (Kelly *et al.*, 1999). Moreover, de-fluorinating to form sidewall aminoalkyl-functionalized nanotubes was found (Mickelson *et al.*, 1998 and 1999). In various alcohol solvents, these functionalized SWNTs were solvated as individual tubes, making it possible to carry out further solution chemistry. There are various organic functionalizations, for example, Pekker *et al.*, 2001 reported the hydrogenation of carbon nanotubes via the Birch reduction in ammonia. Other examples include the derivatization of small diameter (ca. 0.7 nm) SWNTs reported by Tour *et al.*, 2001, the interactions with anilines reported by Wilson *et al.*, 2001, the reactions with nitrenes, carbenes, and radicals reported by Hirsch *et al.*, 1998, 2001 and the 1,3-dipolar addition reported by Prato *et al.*, 2002. Furthermore, direct addition to the unsaturated π-electron systems of SWNTs can also occur through such as the [2+1] cycloaddition of nitrenes, [4+2] Diels-Alder cycloaddition of 0-quinodimethane performed under microwave irridation, cyclopropanation accomplished under Bingel reaction conditions that can be visualized using STM. These functionalizations break the nanotubes bundles, which is essential to the solubility. Solubilized carbon nanotubes were used as starting materials for further chemical and biological modification. The fabrication of polymeric carbon nanocomposites (Star *et al.*, 2001; Ajayan *et al.*, 2001) experimentally prepared and fabricated the designing of the optical application, the probing of nanotubes-molecule interactions, and the conjugation with biological species, especially protein.

The main factor was used to explain the reactivity of the tube being a pyramidalization angle. The reactivity of the fullerenes is primarily driven by the enormous strain engendered by their spherical geometry as reflected in the pyramidalization angles of the carbon atoms (Haddon, 1993). For an sp^2-hybridized (trigonal) carbon atom, planarity is strongly preferred, and this implies a pyramidalization angle of $\theta_P = 0°$, whereas an sp^3-hybridized (tetrahedral) carbon atom requires $\theta_P = 19.5°$ (Figure 4a). All of the carbon atoms in [60]-fullerene have $\theta_P = 11.6°$, and it is immediately clear that their geometry is more appropriate for tetrahedral than trigonal hybridization. Thus, the chemical conversion of any trivalent carbon atom in [60]-fullerene to a tetravalent carbon atom relieves the strain at the point of attachment and mitigates the strain at the 59 remaining carbon atoms (Haddon, 1993). Hence, reactions that serve to saturate the carbon atoms are accelerated by strain relief, and this strongly favors fullerene addition chemistry (Haddon, 1993; Taylor *et al.,* 1993).

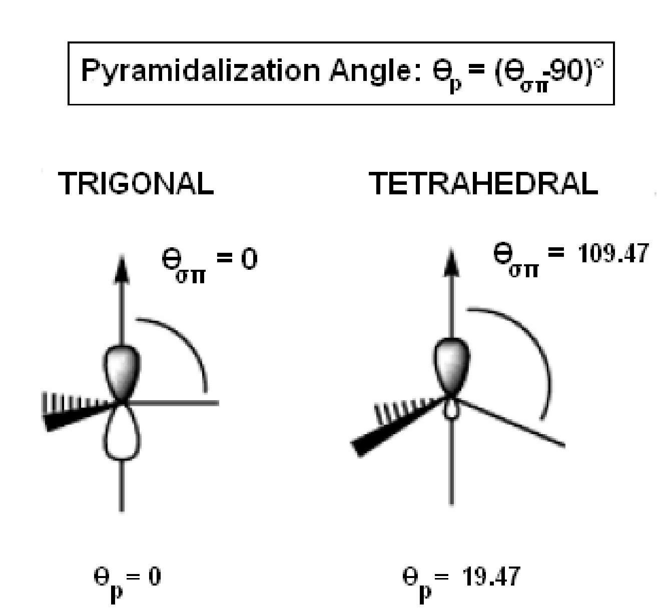

Figure 6 Diagrams of pyramidalization angle (θ_P)

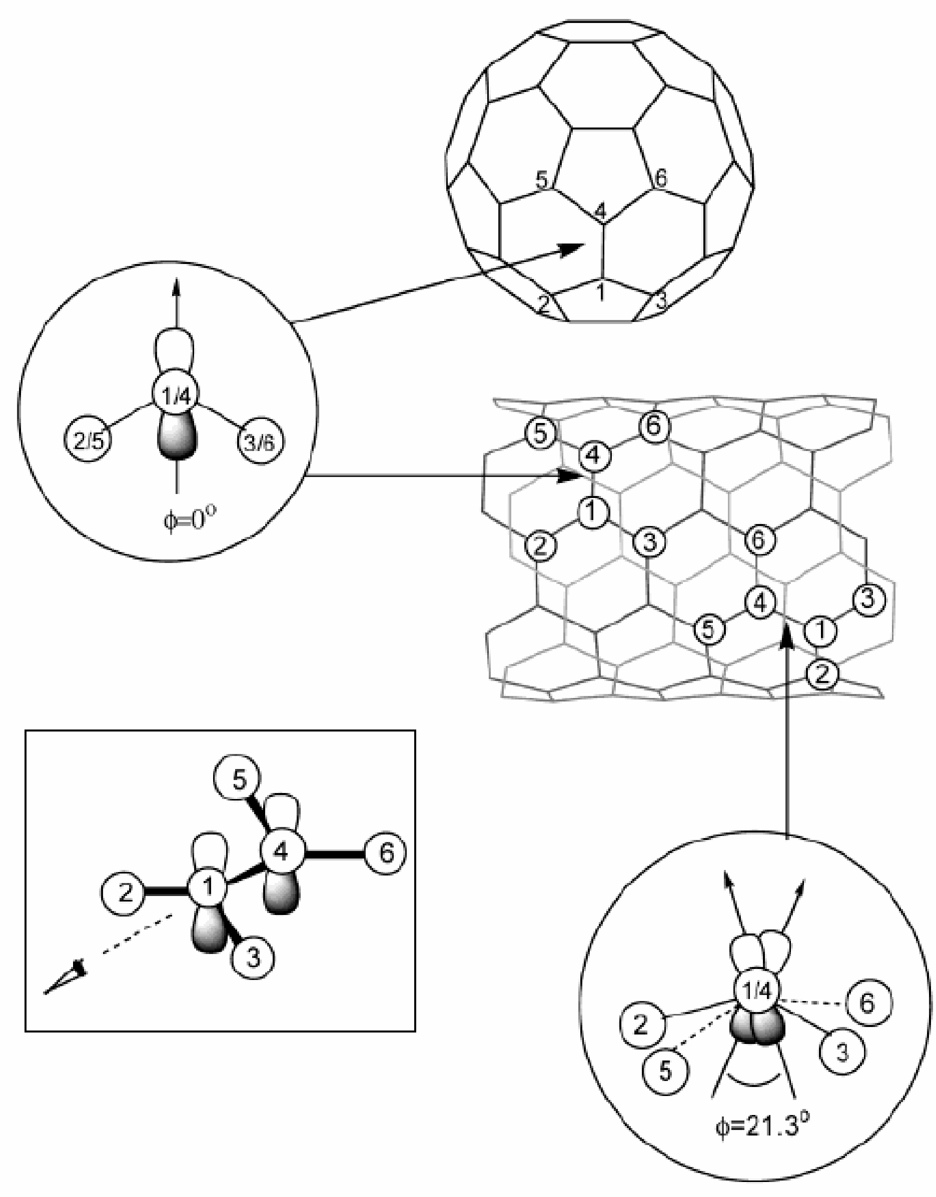

Figure 7 Diagrams of the π-orbital misalignment angles (Φ) along the C1-C4 in the [5,5] SWNT and its capping [60]-fullerene.

Furthermore, the curvature-induced pyramidalization and misalignment of the π-orbitals (Hamon, *et al.,* 2001; Chen, *et al.,* 1998; Haddon, 1993) of the carbon atoms induces a local strain (Figure 4b), and carbon nanotubes are expected to be more reactive than a flat graphene sheet. From the standpoint of chemistry, it is conceptually useful to divide the carbon nanotubes into two regions: the end caps and the side wall. The end caps of the carbon nanotubes resemble a hemispherical fullerene, and because it is impossible to reduce the maximum pyramidalization angle of any fullerene below about θ_P max = 9.7°, (Haddon, 1997) this ensures that the end caps will always be quite reactive, irrespective of the diameter of the carbon nanotube. In the [5,5] SWNT, which is capped by a hemisphere of [60]-fullerene, the pyramidalization angles are as follow: $\theta_P = 11.6°$ (end cap) and $\theta_P = 6.0°$ (side wall) (Hamon, *et. al.,* 2001).

H. C. Brown and B. C. Subba Rao *et al.* (1956), reported first in 1956 that the hydroboration in a clear solution of sodium borohydride-aluminium chloride in diglyme reacts readily with olefins at room temperature and in 1957 that olefins may be readily converted into organoboranes under mild experimental conditions, as indicated by the reaction which has provided a major new route to these interesting derivatives:

$$9RCH = CH_2 + 3NaBH_4 + AlCl_3 \longrightarrow 3(RCH_2 - CH_2)_3B + AlH_3 + 3NaCl$$

$$12RCH = CH_2 + 3NaBH_4 + BF_3 \longrightarrow 4(RCH_2 - CH_2)_3B + 3NaBF_3$$

$$6RCH = CH_2 + B_2H_6 \longrightarrow 2(RCH_2 - CH_2)_3B$$

In these hydroborations, the boron atom adds to the less substituted carbon atom, with the hydrogen atom adding to the more substituted carbon atom of the double bond. The organoboranes are rapidly oxidized by alkaline hydrogen peroxide to the corresponding alcohols. Consequently, hydroboration followed by oxidation provides a convenient route for the anti-Markownikoff hydration of double bonds. In addition, the hydroboration is both high regioselectivity (regioselectively?) and stereoselectivity (stereoselectively?). From the quantum chemical calculation, the reaction mechanism disclosed is as shown in Scheme 1. This reaction is initiated by the electrophilic attack of the electron-deficient boron center of borane to the π-bond of ethylene, forming a π-complex followed by B-H breakage (Sunderg *et al.*, 1979; Nagase *et al.*, 1980; Wang *et al.*, 1990). Recently, hydroboration of ethylene with borane was investigated using B3LYP/6-31G(d) (Lu *et al.*, 2003). It predicted no activation energy for the overall reaction, and was in agreement with the previous kinetic experimental report of Pasternack *et al.*, 1988 with the negative activation energy -4 kcal/mol. Later, the *ab initio* SCF calculations overestimated the activation > 4 kcal/mol (Nagase *et al.*), MP2 calculations with inclusion of the correlation energy found no transition state for the reaction (Wang *et al.*). In the gas phase, the B3LYP/6-31G(d) calculations agree with the predicted reaction mechanism, but differ largely in the predicted energetics. The B3LYP/6-31G(d) prediction is superior to the previous *ab initio* SCF calculations regarding the energetics of hydroboration with ethylene.

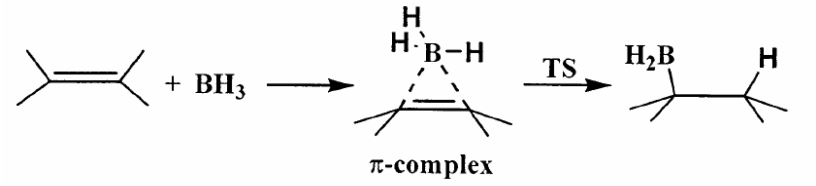

Figure 8 Hydroboration reaction of olefin with borane**.**

The hydroboration reaction of fullerene (C_{60}) in the experimental report (Henderson *et al.*, 1996) was found to be facile, it being of high site selectivity which occurs at the 6,6 ring fusion C=C bond of C_{60}. That latter finding is rather encouraging not only because it led to functionalized C_{60} but also because its organoborane can be rapidly converted into hydrogenated products, observed ΔG = 1.4±0.2 kcal/mol, which is an example of a wide variety of organic transformations. The ONIOM(B3LYP/6-31G(d):AM1) calculation was employed to predict the hydroboration of fullerene. It found that BH_3+C_{60} is exothermically (-15.1 kcal/mol), in agreement with the full optimization on B3LYP/6-31G(d) level (-15.0 kcal/mol). The study shows that ONIOM(B3LYP/6-31G(d):AM1) is reliable. However, the hydroboration of fullerene is neither kinetically nor thermodynamically favorable over that of ethylene owing to the electron deficiency of C_{60}. Furthermore, the hydroboration of the sidewalls of (5,5) SWNTs was predicted to be thermoneutral using ONIOM(B3LYP/6-31G(d):AM1), which would not occur readily. Previously, Lu et al. reported several theoretical studies of the functionalization of SWNTs by applying ONIOM, including the cycloaddition of several 1,3-dipolar molecules (2002 and 2003), epoxidation (2002), Diels–Alder cycloaddition (2002) and [2+3] cycloaddition (2002) onto the sidewall of nanotubes. Mostly, B3LYP/6-31G* at the high-level, and a semiempirical AM1 approach for the low-level real SWNT, was applied to predict the reaction energy and activation energy. Furthermore, our previous studies had been successfully accessed by the ONIOM method (Warakulwit *et al.,* 2005) and zeolites (Namuangruk, *et al.,* 2004; 2005) where the different levels of theory are applied to different parts of a molecule. Within the framework, the modified handling of like atoms is introduced to terminate the dangling bonds of the model system.

From our knowledge, if a single-walled carbon nanotube (SWNT) is doped with either B or N, the electronic properties will be different from those of bulk doped-graphite. The quantum confinement and curvature of the cylinders will result in novel electronic, mechanical, and chemical properties, which are also different from their undoped counterparts. In particular, substitutional doping of B and N within graphene nano-cylinders will introduce strongly localized electronic features in the valence or conduction bands, respectively, and will enhance the number of electronic states at the Fermi level depending on the location and concentration of dopants. Little work has been carried out in doping SWNTs with either B or N, but we believe that these systems should exhibit unusual quantum effects, and it should be possible to tailor the band gaps of semiconducting SWNTs when doping at very low concentration levels. Therefore, experimental and theoretical work is needed in order to exploit the possibility of doping quantum carbon wires. This review is targeted to motivate a new field in nanotube science, thus breaking new ground in the physics and chemistry of one-dimensional carbon systems. There are numerous challenges that we must overcome before producing N- and B-doped SWNTs in a controlled way, but it is clear that these materials will be important in the fabrication of nanotube composites, electronic devices, sensors, nanobots, etc. In addition to SWNTs, it is also possible to dope double-walled (DWNTs) and multi-walled nanotubes (MWNTs) with B and/or N. In these systems, the electronic and mechanical properties change and new electronic, mechanical, and vibrational effects could be observed.

From the theoretical point of view, Hernandez *et al.*, 1999 have described the mechanical properties of CNx and CBx nanotubes demonstrating that high concentrations of B and/or N within SWNTs lower the Young's modulus. Nevertheless, the Young's modulus values still remain in the order of 0.5-0.8 TPa. This phenomenon has been experimentally confirmed in pristine and N-doped MWNTs. Unfortunately, the experimental values are quite different from the theoretical ones. For example, the Young's modulus for pristine and N-doped MWNTs are 0.8-1 TPa and ~30 GPa, respectively. We believe that the low values observed for N-doped nanotubes are the result of the relatively high N concentration (e.g. 2-5%) within the tubes, which introduces defects and lowers the mechanical strength. If the N concentration is <0.5%, it is expected that the mechanical properties will not be substantially altered (impaired?).

B has one electron less than C, and when it substitutes for C atoms within a SWNT (three-coordinated B) sharp localized states below the Fermi level (valence band) appear. These states are caused by the presence of holes in the structure, and the tube could be considered as a p-type nano-conductor. From the chemical standpoint, this structure would be more likely to react with donor-type molecules.

For N-doped SWNTs, two types of C-N bonds could occur in CNTs. The first is a substitutional N (N coordinated to three C atoms in an sp2-like fashion), which induces sharp localized states above the Fermi level because of additional electrons, which are injected into the structure. These types of tubes exhibit n-type conduction, and are more likely to react strongly with acceptor molecules. The second type is a pyridine-type N (two coordinated N), which can be incorporated into the SWNT, provided that a C atom is removed from the framework. This type of defect induces localized states below and above the Fermi level. Therefore, substitutional N doping in SWNTs should result in n-type conducting behavior, whereas pyridine-type N may produce either a p- or n-type conductor, depending on the doping level, the number of N atoms, and the number of removed C atoms within the hexagonal sheet. In order to observe genuine quantum effects in doped CNTs, dopants must be present within SWNTs of a narrow diameter (<1-2 nm).

For synthesis of doped nanotubes, boron doping can be carried out by growing tubes in a carbon arc using a BN-rich consumable anode (Carroll *et al.,* 1998). On the other hand, nitrogen-doped carbon nanotubes can be synthesized by pyrolyzing ferrocene/melamine mixtures at elevated temperatures (Czerw *et* *al.,* 2001). Changes in the electronic structure of carbon nanotubes due to the introduction of boron and nitrogen in the lattice have been identified using scanning tunneling spectroscopy (Carroll *et al.,* 1998; Czerw *et al.,* 2001). B and N substitution reactions: B- and N-doped SWNTs can also be produced using partial substitution in the presence of B_2O_3 vapor and N_2 at 1500-1700 K (Golberg et al., 2000). In these experiments, B-doped tubes exhibit a B/C ratio of <0.1. Lower amounts of N (N/C <0.01) can also be incorporated within the hexagonal framework (Golberg et al., 2000). In contrast to B-doped MWNTs, SWNTs do not exhibit preferred chiralities, possibly because the dopants only substitute individual C atoms within the framework, thus preserving the tubule chirality. It is noteworthy that both B- or N-doped SWNTs show corrugation, attributable to defects on the C surface. Carroll *et al.,* (1998) showed both boron- and nitrogen-doped tubes are metallic with no apparent band gap, in contrast to undoped tubes with varying electronic character. However, in both cases, the local density of states (LDOS) exhibit either strongly localized acceptor states (p-doping) or donor states (n-doping) near the Fermi level. First principles calculations show that changes in the LDOS of boron-doped tubes, as determined from tunneling microscopy, must be interpreted in terms of nanodomains of BC_3 islands. However, pyridine-like N structures are responsible for the metallic behavior and the strong electron donor states observed near the Fermi level in the LDOS of nitrogen-doped tubes (Czerw *et al.,* 2001). The temperature-dependent thermoelectric power of boron- and nitrogen-doped carbon nanotubes have been measured, showing that such dopants can be used to modify the majority carrier conduction from p-type to n-type. These electrons-(hole)-rich structures are examples of n-type (p-type) nanotubes, which could again pave the way to real molecular heterojunction devices (Choi *et al.,* 2000). As noted above, oxidative doping during nitric acid purification exerts a noticeable effect on the electronic transitions seen in the SWNTs. Compared with un-doped carbon nanotubes, it is expected that the BN-doped nanotubes have many novel electronic, mechanical, conductive and optical properties, and thus possess potential applications in many fields, such as nanosized photonic and electronic devices, superhard materials, electron field emitters, and sensitive sensors. The lithium absorption energies and electronic structures of boron- or nitrogen-doped single-walled carbon nanotubes (SWNTs) were investigated using first-principles calculations. B-doping decreases lithium absorption energy dramatically both at inner and outer sites. B-doping forms an electron-deficient structure in SWNTs, which can stabilize the Li absorption on the tube walls; however, N-doping forms an electron-rich structure, and will hinder the Li absorption in SWNTs. The calculations suggest that B-doping in SWCNT will improve its Li absorption performance (Zhou *et al.*, 2004). Theoretical investigations on boron and nitrogen-doped zigzag single-walled carbon nanotubes carried out to explore the capability of the nanotubes to incorporate Li+ ion in its interior, and found that the BN-doped nanotubes have higher interaction energies with lithium cation than the pure nanotubes (Quinonero *et al.*, 2005). In a recent theoretical study (Zhang *et al.*, 2006), the geometries and stabilities of mono-BN doped (5,5) armchair SWNTs are first investigated by AM1 and HF/4-31G methods. The calculations suggest that both methods obtain similar results. Their calculation considered B and N atoms substitution at the C atom at various positions along the tube. In addition, exchanging the position of two heteroatoms in each isomer would be investigated. Both methods suggested that mono-BN doped isomer, B and N atoms prefer to stay together. In addition, mono-BN doped isomer, B and N atoms liked to locate at the sloppy bond (or 1,3 pair site on sidewalls of SWNTs) more than 1,2-pair site in the thermodynamic limit, which perhaps is that these neighbored BN atoms doped SWNTs make the affluent electrons on the N atom transfer more easily to the B atom than the two disconnected BN atoms.

MATERIALS AND METHODS

An accurate determination of the mechanisms of SWNTs functionalization is computationally extremely demanding due to the size of such nanosystems. The Our own N-layered Integrated molecular Orbital molecular Mechanics (ONIOM) (Morokuma *et al.*, 1995) is a computationally efficient tool for the study of chemical reactions involving large molecular systems. This is achieved by allowing a partitioning of the molecule (real) into two or three different regions, where a high-level calculation on a small region (model) is performed, and the effects of the remainder spectator regions are included at a low-level of theory. The dangling bonds of the model fragment at the boundary between different levels are saturated with hydrogens as link atoms. Selection of the atoms in the model and the level of theory in that part of the system (high-level), as well as the level of theory for the real system (low-level), are the factors regulating the accuracy of the results.

Details of Calculations

The two-layered ONIOM scheme, was used to investigate the hydroboration reaction onto the sidewalls of SWNTs because the size of the system prevents the use of *ab initio* calculation. The semiempirical AM1 method (Dewar, 1977), and the hybrid density functional B3LYP method (Becke, 1993 and Lee Yang Parr, 1988) were employed for the low level and high level treatments, respectively. The (5,5) armchair SWNT ($C_{130}H_{20}$) (diameter ≈ 6.8 Å, in Figure 9a) represented the structural model tube, in which the high level part is a C_{16} cluster (see the shaded atoms in Figure 9a), together with ten H-atoms as boundary atoms (not shown in Figure 9). The high-level part was treated with the standard 6-31G(d) basis set, except C1 and C2, carbon reactive centers and the borane molecule (BH_3) which were treated with the B3LYP/6-31++G(d,p) method. Two types of inequivalent C-C pair sites, i.e., 1,2 pair site and 1,3 pair site, on the (5,5) armchair SWNTs is shown in Figure 9. the 1,2 pair site is generally more reactive than the 1,3 pair site, hence, we have considered only the 1,2 pair site for functionalization of SWNTs with hydroboration reaction.

In this study, we investigate the effect of boron and nitrogen atoms onto (5,5)-armchair sidewall of SWNTs in the hydroboration reaction by substitution of boron and nitrogen atoms nearby the carbon reactive center C1 and C2 atoms. From the structural geometry of the high level of the sidewalls of SWNTs in Figure 9b, there are two different configurations which are the boron atom and the nitrogen atom situated near the C1-C2 reactive center defined as: BN-doped SWNTs and NB-doped SWNTs, as shown in Figures 9c and 9d, respectively. BN-doped SWNTs (Figure 9c) is where the B atom was located near the carbon reactive site of C2. We substituted B at the location of C3 and replaced the N atom at the C4 position, so the high level part composed of

C1C2B3N4 (Figure 9c). On the other hand, the NB-doped SWNTs (Figure 5d) is where the N atom was located near the reactive site of C2. We substituted the N atom at the location of C3 and the B atom replaced the C4 position, so the high level part was set into C1C2N3B4 (Figure 9d).

Furthermore, we classified the C-C bonds into two types: the circumferential bond, c, which is the C-C bond running parallel to the circumference of tube; and the axial bond or sloppy bond, a, as noted in Figure 9b. This figure shows the two different types of bond when the mono-BN atoms are doped into the sidewalls of (5,5) armchair SWNTs. As a result, BN-doped SWNTs could be divided to two types of geometries: BN-doped, when the mono-BN atom is situated at the circumferential bond, c as noted BN-doped (c) (Figure 9c), and BN-doped when the mono-BN atom is located at the axial bond, a as noted BN-doped (a) (Figure 9e). Such NB-doped SWNTs, NB-doped when the mono-BN atom is situated at the circumferential bond, c as noted NB-doped (c) (Figure 9d) and NB-doped when the mono-BN atom is located at the axial bond, a as noted NB-doped (a) (Figure 9f).

During the structure optimization, the whole structure of SWNTs and the adsorbate are allowed to relax. Frequency calculations were carried out to confirm the single imaginary mode for all transition states. The optimized C1-C2 bond distances are about 1.391, 1.396, and 1.396 Å, for the perfect tube, the BN-doped tube, and NB-doped tube, respectively.

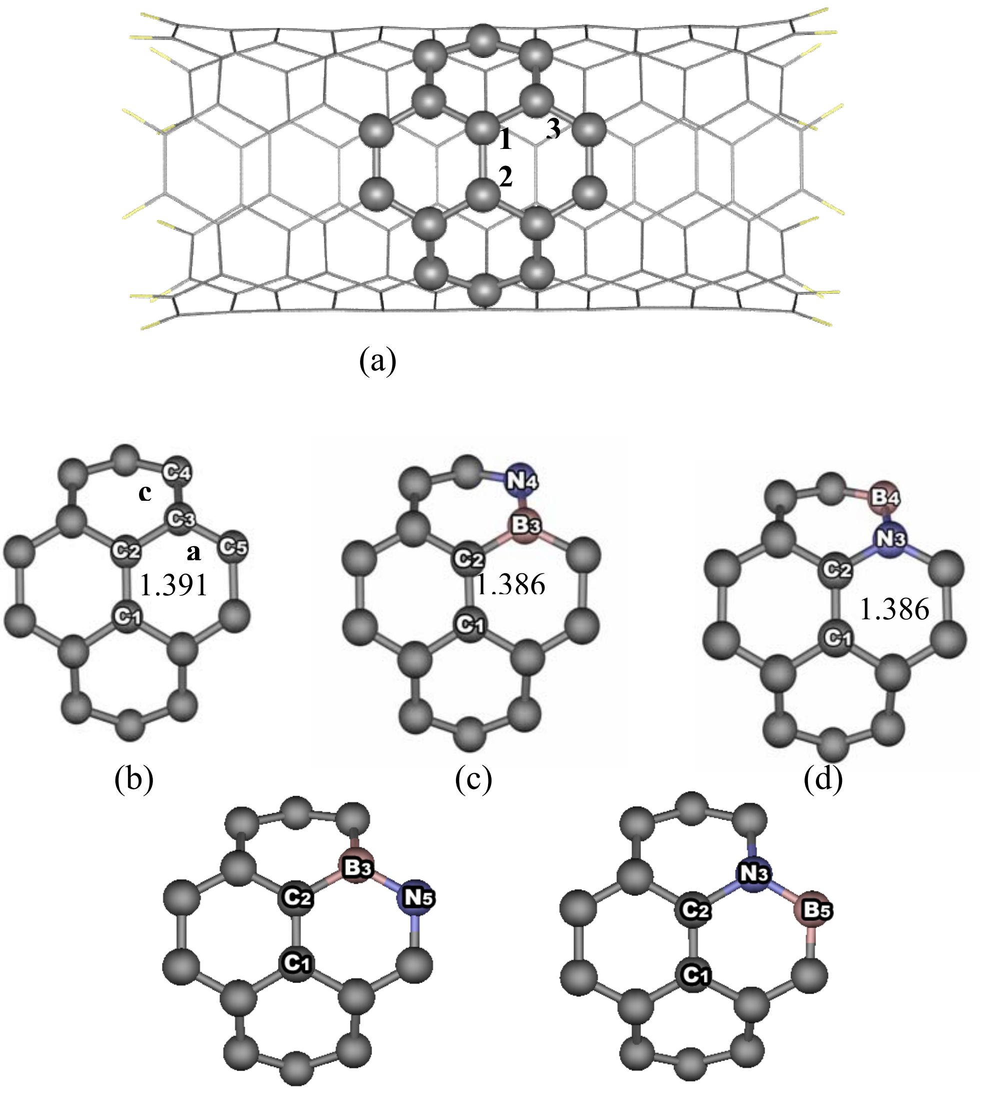

(a)

(b) (c) (d)

(e) (f)

Figure 9 a) The ONIOM model of (5,5) SWNT ($C_{130}H_{20}$ cluster) and five separate model systems: b) perfect, C1C2C3C4 c) BN-doped(c) at the circumferential bond, C1C2B3N4 (d) NB-doped (c) at the circumferential bond, C1C2N3B4 e) BN-doped (a) at axial the bond, C1C2B3N5 (f) NB-doped (a) at the axial bond, C1C2N3B5. Atoms belonging to the quantum cluster (B3LYP) region are drawn as balls and sticks; the rest is treated at the AM1 level of theory.

To understand the effect of the doping of boron and nitrogen atoms onto the sidewall of nanotubes, the systems have been analyzed via the NBO analysis (Natural Bond Orbital) in partitioning schemes applied to B3LYP/6-31++G(d,p) to describe a distribution of charge. The interaction between a donor molecule and an acceptor molecule was analyzed by the natural bond orbital analysis (NBO) .The energetic stabilization due to donor–acceptor interactions can be estimated by the second-order perturbation theory:

$$\Delta E^{(2)}_{\pi_{C1=C2}\rightarrow\sigma^*_{B1}} = -2\frac{\langle \pi_{C1=C2}|\hat{F}|\sigma^*_{B1}\rangle^2}{\varepsilon_{\sigma^*_{B1}}-\varepsilon_{\pi_{C1=C2}}}$$

where is the filled (donor) orbital, * is the unfilled (acceptor) orbital

F the Fock operator,

ε and ε *are the NBO orbital energies of donor and acceptor orbitals.

The quantity of charge *q* transferred associated with interactions between donor and acceptor orbitals is:

$$q \cong \frac{\left|\Delta E^{(2)}_{\pi_{C1=C2}\rightarrow\sigma^*_{B1}}\right|}{\varepsilon_{\sigma^*_{B1}}-\varepsilon_{\pi_{C1=C2}}}$$

$\sim 10^{-3}$ e which is typically much less than that required for formation of an ion pair.

In all cases, geometries were fully optimized without any symmetry constraints performed within the two-layered ONIOM (B3LYP:AM1) approach using the Gaussian 03 program.

RESULTS AND DISCUSSION

The substitution of boron and nitrogen atoms near the carbon reactive center, C1-C2 bond at the different bonds; circumferential, c and axial, a bonds of bare BN-doped SWNTs and bare NB-doped SWNTs.

The optimized BN-doped and NB-doped onto the sidewalls of (5,5) armchair SWNTs at two different bonds using the ONIOM(B3LYP:AM1) predicted the heat of formation in the unit of au as shown in Table 1. The results demonstrate that the substitution of mono-BN atoms at different bond types of both BN-doped SWNTs and NB-doped SWNTs prefers to occur at the axial bond, (a) of the tube which could stabilize the tube as shown in the lower heat of the formation energy in the unit of au and the relative energy compared with the doping of mono-BN atoms at the circumferential and axial bonds, ΔE kcal/mol, to be -15.6 kcal/mol for BN-doped SWNTs and -37.5 kcal/mol for NB-doped SWNTs, respectively.

For our systems, the hydroboration reaction with SWNTs, is predicted by the optimized organoborane products of all types of SWNTs, as shown in Table1, in the reaction energy, Er (kcal/mol) using ONIOM(B3LYP:AM1). The reaction energies of mono-BN atoms at the circumferential bond provide the more stable organoborane product, as shown in Table1, of Er in kcal/mol. For BN-doped SWNTs at the c bond gives a higher exothermicity of hydroborations, -5.4 kcal/mol, comparable with BN-doped at a bond, -2.3 kcal/mol. This is the same evidence of the NB-doped at c bond which provides a more stable product, Er = -3.3 kcal/mol, while a less stable product 23.2 kcal/mol in Table1.

From the study, we selected the model of mono-BN atoms at the circumferential bond to further study in our systems as we considered it to be the more reactive substance for the hydroboration reaction and would give more stable organoborane products.

TABLE 1 The heat of formation (HF) in the au unit of bare BN-doped SWNTs and bare NB-doped SWNTs, the relative energy of bare BN-doped SWNTs and NB-doped SWNTs as noted in ΔE (kcal/mol), and the reaction energy of the hydroboration reaction, Er (kcal/mol) on the sidewall of SWNTs in which mono-BN atoms were doped into different bonds; the circumferential bond, c and axial, a of tubes.

System	BN-doped SWNTs		NB-doped SWNTs	
	c	a	c	a
HF[1] (au)	-617.64952	-617.67437	-617.67097	-617.73072
ΔE[2] (kcal/mol)	0.0	-15.6	0.0	-37.5
Er[3] (kcal/mol)	-5.4	-2.3	-3.3	+23.2

[1] HF = Heat of Formation in au unit.

[2] ΔE (kcal/mol) = the heat of formation energy of each bare tube between mono-BN atoms at the circumferential bond, c and mono-BN atoms at the axial bond
= HF (mono-BN at a bond of SWNTs)- HF (mono-BN at c bond of SWNTs)

[3] Er = Reaction energy of the addition of BH_3 to the tube.
= $E_{product} - (E_{tube} + E_{BH3})$

1. The hydroboration reaction of the perfect sidewall armchair (5,5) SWNT ($C_{130}H_{20}$, C1C2C3C4) with borane

The important geometric parameters of the optimized reactant, transition state and product of the hydroboration reaction are depicted in Figures 10a and 10d, respectively. The only one imaginary frequency proved the optimized saddle points as being the true transition state structure. The reaction gives an organoborane product of BH_2 adspecies and –H species connecting to the neighboring carbon atoms (Fig. 10d). The product of hydroboration onto armchair SWNTs differs from that of ethylene and is unique. The $–BH_2$ and –H adspecies (in Figure 10d) is 1.671 Å as the result the C1-H1 bond being elongated to 1.142 Å. The C1=C2 reactive site in its product is elongated from 1.391 Å to 1.671 Å, which is an ordinary range of single bonds of most chemical functioalizations. It demonstrates that the adopted sp^2 hybridized to sp3 in order to relieve the strain. Furthermore, the reaction energy and activation energy of the hydroboration of (5,5)-armchair SWNTs are predicted to be -0.95 and 11.35 kcal/mol, respectively. The results show that this could occur via the high barrier energy but provide a less stabilized product owing to the terms of translational entropy. We can conclude that the hydroboration reaction on the perfect sidewalls of (5,5) armchair SWNTs could not prefer to occur facile due to the slight exothermic. Our results from ONIOM (B3LYP:AM1) calculations and previous work by Long *et al.* agree well in the predicted reaction mechanism but differ slightly in the predicted energies for the reason that the whole of the optimized structure in our study was allowed to relax. It is noticeable that the adsorbed geometry is not found. Undeniably, the adsorption molecule could not facilely take place because carbon nanotubes possess a high chemical stability and electron deficiency character, although the π bond is considered, which is reasonably attracted toward borane.

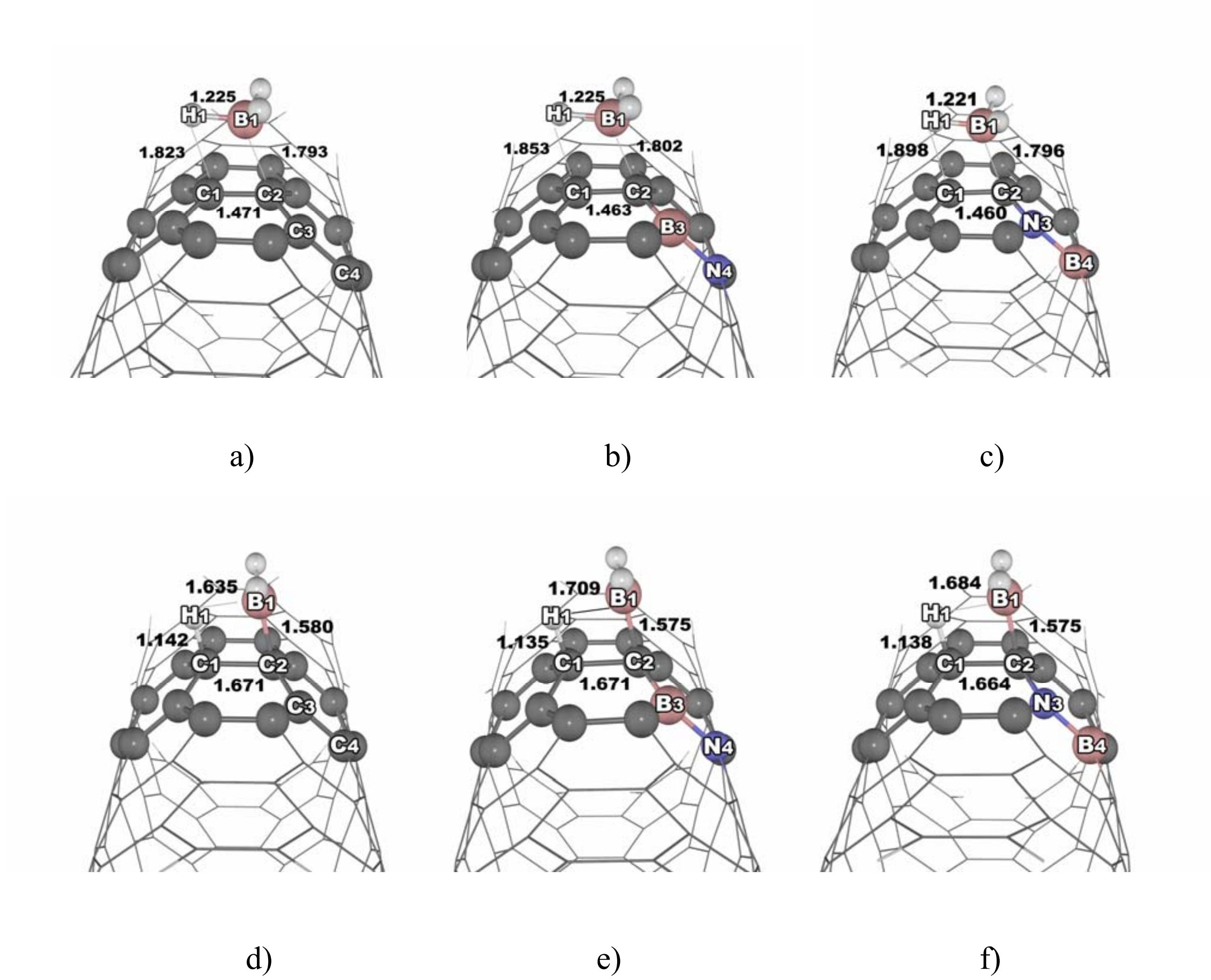

Figure 10 The selected parameters (bond length in Å) obtained at the ONIOM(B3LYP:AM1) level of theory for the transition states (a,b,c) and the products (d,e,f) of the hydroboration reaction of the perfect sidewall of 5,5-armchair SWNT fragment ($C_{130}H_{20}$, C1C2C3C4); BN-doped sidewall of 5,5-armchair SWNT fragment ($BNC_{128}H_{20}$, C1C2B3N4); and NB-doped sidewall of 5,5-armchair SWNT fragment ($NBC_{128}H_{20}$, C1C2N3B4) with borane, respectively.

The mechanism was clarified by the energy path way of the hydroboration of the perfect sidewall armchair (5,5) SWNT which was scanned by the QST3 method in 9 steps (1-9), as shown in Figure 11. The reaction path is related to a concerted mechanism via an activation barrier 11.35 kcal/mol. The plots of the optimized geometries have shown an energy maximum at step number 6 (Figure 11a), corresponding to a true transition state which gave the same structure as the transition state in performing the optimization with the keyword OPT=TS shown in Figure 10a. Figure 11 is the plot to illustrate the lengthening of bonds C1-C2, and H1-B1, and the shortening of the bonds C1-H1, and C2-B1, which are the significant parameters in the hydroboration reaction. The results from the QST3 method agrees with the adsorbed geometry not found.

To describe the reaction step, the C2-B1 bond initially formed relating to the NBO analysis charge. Borane (BH_3) is a strong electrophile possessing a vacant p-orbital and a positive charge on the boron atom (+0.30). The result was that it could be attached easily by the C-C π bond (onto the 1,2 pair site) of the sidewalls of SWNTs to form the C2-B1 bond. Consequently, the four-centered transition state (Figure 10a) occurs, which are partially charged and ascribed in Table 2. In this step, the electron of the H1-B1 bond transfers to C1 by the appearance of the H1-C1 bond and the coincidence of the cleavage of C1=C2, H1-B1 bond. Finally, it gives an organoborane product of $–B1\text{-}H_2$ adspecies connecting to C2 of the reactive site onto carbon nanotubes and H1 species linking to C1 of that onto the tube. It is found that carbon nanotubes play a key role on both the electron donor and the electron acceptor for the hydroboration reaction onto the perfect sidewall of armchair (5,5) SWNTs via an asynchronous concerted mechanism, as shown in the electron density difference plots for perfect SWNTs as shown in Figure 12a. The electron density plot of the transition state, already obtained by the ONIOM method confirmed that the hydroboration reaction via an asynchronous concerted reaction by the appearance of the C2-B1 bond, while the H1-C1 bond was not found.

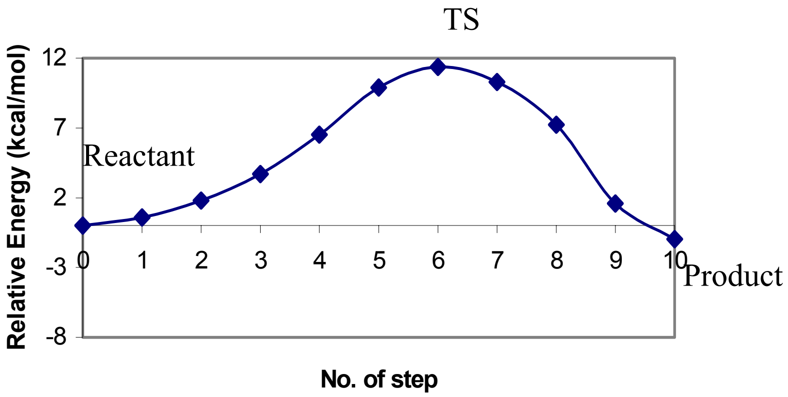

(a)

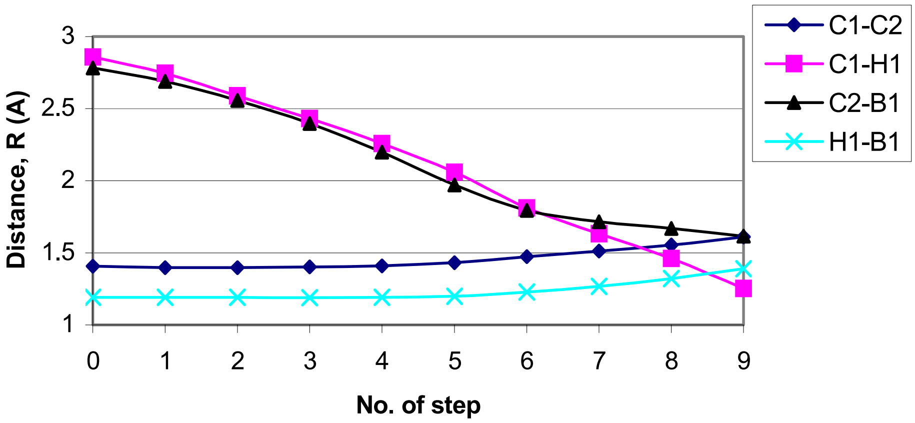

(b)

Figure 11 (a) The reaction path of the hydroboration reaction of perfect sidewall SWNTs plotted between the number of reaction steps and the relative energy (kcal/mol), which was calculated by the QST3 method using the ONIOM(B3LYP:AM1) level of theory. (b) Each step of the hydroboration reaction along the C1-C2, C1-H1, C2-B1, and H1-B1 distance values starting from the adsorbed molecules to the organoborane product path.

TABLE 2 The atomic charge distribution calculated from the natural population analysis (NPA) of the reactant (tube and borane molecule (BH3) and transition state (TS)

Perfect SWNTs			BN-doped SWNTs			NB-doped SWNTs		
q	Reactant	TS	q	Reactant	TS	q	Reactant	TS
C1	-0.02	0.02	C1	-0.01	0.03	C1	-0.05	0.02
C2	-0.02	-0.17	C2	-0.34	-0.49	C2	0.22	0.06
C3	-0.05	0.00	B3	0.75	0.84	N3	-0.57	-0.56
C4	-0.21	-0.21	N4	-0.78	-0.78	B4	0.54	0.54
H1	-0.10	0.12	H1	-0.10	0.11	H1	-0.10	0.10
B1	0.30	-0.22	B1	0.30	-0.23	B1	0.30	-0.23
H	-0.10	0.02	H	-0.10	0.02	H	-0.10	0.02
H	-0.10	0.02	H	-0.10	0.02	H	-0.10	0.03

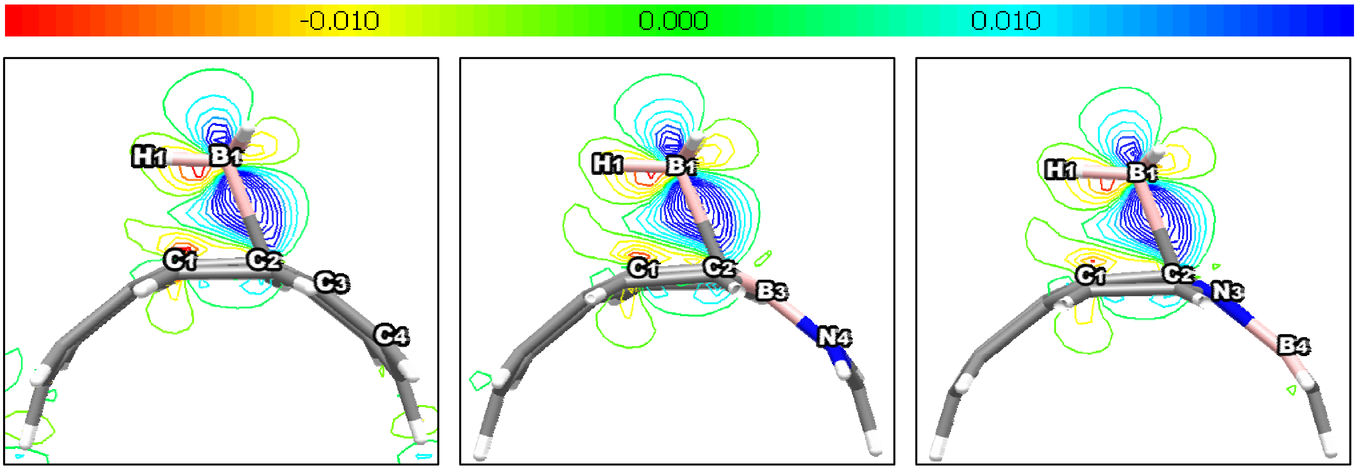

(a) (b) (c)

Figure 12 The electron density plot of the transition state of (a) perfect sidewall SWNTs, (b) BN-doped SWNTs, and (c) NB-doped of SWNTs.

2. The hydroboration reaction of the doping with B,N atoms onto the sidewall armchair (5,5) SWNT ($C_{130}H_{20}$) with borane

To enhance the reactivity of the sidewall of SWNTs we will introduce the defect of B,N-doped onto the sidewall of SWNTs by replacing the B and N atoms to adjacent carbon atoms nearby the C1=C2 bond reactive site. We found that there are two possibilities of B and N atoms substitution that give different results.

2.1 The hydroboration of BN-doped (5,5) armchair SWNTs where the B atom is positioned near the reactive site ($BNC_{128}H_{20}$, C1C2B3N4) with borane

Figures 10b and 10e display the structures and geometric parameters of the transition state and the product of the hydroboration reaction. All of the geometric transition state structures, such as the formation of C2-B1 single bond length and the elongation of B1-H1 bond in the transition state structure are 1.802 and 1.225 Å, respectively. In addition, the C1-C2 bond of the entire product is elongated from 1.386 Å to 1.671 Å, the same as that found in the hydroboration of the perfect sidewall of SWNTs.

Consequently, the activation energy and the reaction energy of the hydroboration reaction of this system are 7.87 and -5.38 kcal/mol, respectively. When comparing the activation energy and reaction energy of the hydroboration of the perfect sidewall of SWNTs to those of BN-doped SWNTs, it is found that the hydroboration of (5,5) BN-doped SWNTs can favorably occur by kinetic and thermodynamic control. The activation energy is reduced by 30%. It is, therefore, concluded that the BN-doped sidewall of SWNTs could encourage the hydroboration reaction.

From the calculation, BN-doped SWNTs were compared to the perfect sidewall SWNT. The calculated C1=C2 bond distance onto the 1,2-pair site obtained in the BN-doped SWNT is slightly shorter (1.386 Å) than that of the perfect one (1.391 Å), as shown in Figure 9c. Moreover, the HOMO-LUMO energy of the BN-doped tube which has been reduced by its HOMO energy is raised and its LUMO energy is lowered (see Table 3). This reveals that the isoelectric B and N doped on SWNTs induced the reduction of the energy gap due to p-type and n-type impurities.

TABLE 3 The HOMO, LUMO, Energy gap (eV), and the relative charge of C1 and C2 at the reactive center from the NPA analysis of the perfect, BN-doped, and NB-doped SWNT.

System	HOMO	LUMO	Eg	NPA Atomic Charge		NPA Relative Charge	
				C1	C2	C1	C2
Perfect SWNTs	-4.20	-2.81	1.39	-0.02	-0.02	0.00	0.00
BN-doped SWNTs	-4.17	-2.89	1.28	-0.01	-0.34	+0.01	-0.32
NB-doped-SWNTs	-4.15	-2.88	1.27	-0.05	+0.22	-0.03	+0.24

The NPA analysis is a descriptor to explain the substitution of boron and nitrogen atoms onto the perfect sidewall of carbon nanotubes to enhance the reactivity of carbon nanotubes in the hydroboration reaction. It makes known the reactivity of the different structural forms of the sidewall of carbon nanotubes. The optimized structure of BN doped SWNTs shows the different charges from the perfect tube since the eletronegativity of B < C <N atom, as a result the charge of the C1-C2 reactive center on the BN-doped SWNTs differs significantly from that of the perfect tube (in Table 3). The charge of C1 of the perfect sidewall of carbon nanotubes as equal as that of C2 (-0.02), whose charge density is slightly negative. As the C2 of BN-doped SWNTs has been

occupied by more electron density (-0.34) than that of the perfect sidewall SWNT (-0.02), when boron is substituted at C3. Moreover, the summary of the NPA charge of BH_3 at the transition state of BN-doped SWNTs is calculated to be -0.08q, which is a more negative value, compared with that of the perfect SWNTs (-0.06q). The BN-doped where the boron is near the reactive center (C1C2B3N4 model) assists the electron transfer from the π-bond of the tube to the vacant p-orbital of borane by increasing the magnitude of the electron transfer. It was shown by $\Delta E^{(2)}_{i\rightarrow j}$ of the π bond to σ* of boron in the borane molecule where the value increased from 7.98 to 9.86 eV, for the perfect SWNTs and BN-doped SWNTs, respectively. The effect of boron and nitrogen atoms is that they support the capability of the electrophilic substance of carbon nanotubes to form a facile four-centered transition state and to stabilize the organoborane product of the BN-doped sidewall of SWNTs when compared with perfect SWNTs. Therefore, the hydroboration reaction of BN-doped SWNT could enhance reactivity of hydroboration and it can occur via the same asynchronous concerted interaction as that of the perfect sidewall of nanotubes as shown in Figure 12b.

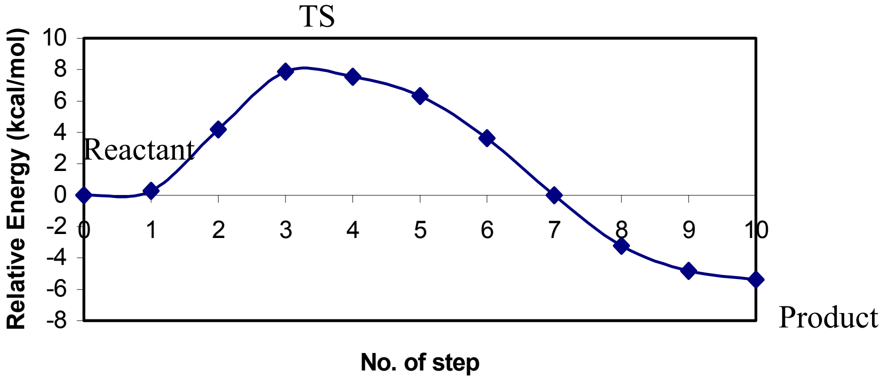

(a)

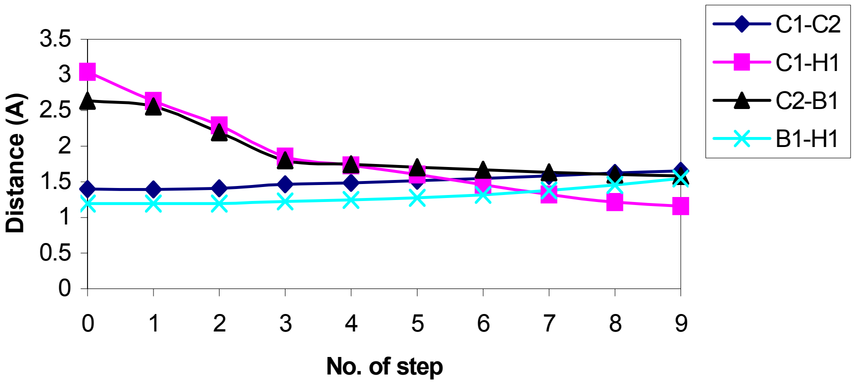

(b)

Figure 13 (a) The reaction path of the hydroboration reaction of the BN-doped sidewall SWNTs plotted between the number of the reaction step and the relative energy (kcal/mol), which is calculated by the QST3 method using the ONIOM(B3LYP:AM1) level of theory, (b) Each step of the hydroboration reaction along the C1-C2, C1-H1, C2-B1, and H1-B1 distance values starting from the adsorbed molecules to the organoborane product path.

2.2 The hydroboration of NB-doped (5,5) armchair SWNTs where the N atom is located near the reactive site ($NBC_{128}H_{20}$, C1C2N3B4) with borane

The hydroboration reaction of NB-doped sidewalls of SWNTs with borane is as an asynchronous concerted mechanism as that of the perfect and BN-doped sidewall of SWNTs. The significant structures and geometric parameters of their transition state and product are depicted in Figures 10c and 10f. These optimized structures and parameters are not quite different from the perfect sidewall but the energy of the transition state and product is more stable than that of the perfect sidewall. The calculated activation barrier (Ea) and the reaction energy (Er) for the NB-doped sidewall of SWNTs with borane are 10.09 and -3.27 kcal/mol, respectively. The NB-doped sidewall of SWNTs could also improve the reactivity of the hydroboration reaction because of the presence of B and N atoms. It was predicted to depend on the position of the doping of B and N atoms.

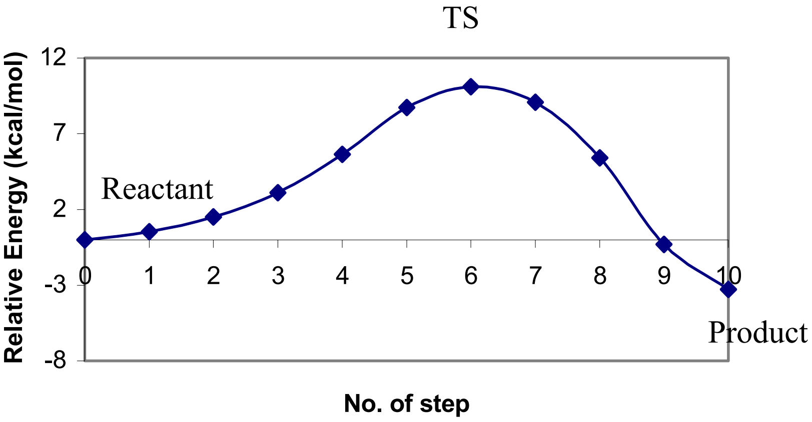

(a)

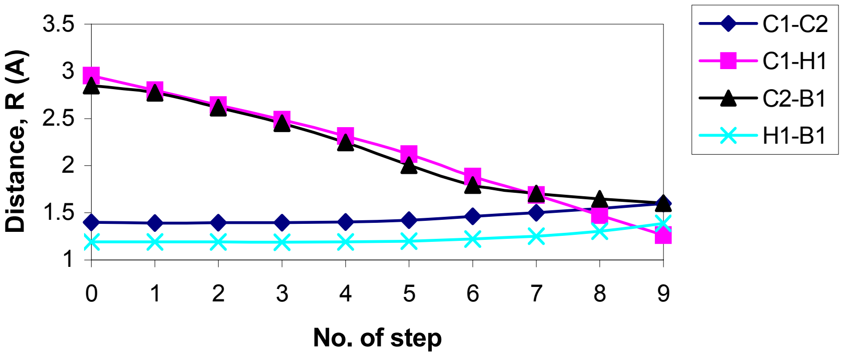

(b)

Figure 14 (a) The reaction path of the hydroboration reaction of the NB-doped sidewall SWNTs plotted between the number of the reaction step and the relative energy (kcal/mol), which calculated by the QST3 method using the ONIOM(B3LYP:AM1) level of theory, (b) Each step of the hydroboration reaction along the C1-C2, C1-H1, C2-B1, and H1-B1 distance values starting from the adsorbed molecules to the organoborane product path.

The NB-doped SWNTs; C1C2N3B4 model was compared to the perfect sidewall SWNT. The calculation of C1=C2 bond distance onto the 1,2-pair site obtained in the NB-doped SWNT also is slightly shorter (1.386 Å) than that of the perfect one (1.391 Å), as shown in Figure 9c. In addition, the energy gap of the NB-doped SWNTs is also reduced by its HOMO energy being raised and its LUMO energy being lowered (in Table 3), which is the same as the result in the BN-doped SWNTs.

From the calculation, it was found that the magnitude of the stabilization energy ($\Delta E_{i \to j}^{(2)}$) of $\pi_{C1-C2} \to \sigma^{*} B(ofBH_3)$ in the NB-doped SWNTs was 8.35 eV which performed the electron transfer from the NB-doped tube to the borane, which was more than that for the perfect tube (7.98 eV) as shown in Table 3. It further showed that NB-doped tube is more reactive in the hydroboration reaction than in the perfect tube.

Table 4 The NBO analysis represented the magnitude of transferred electron and stabilization energy for borane functionalized on high level of perfect, BN-doped, NB-doped SWNTs calculated at B3LYP/6-31++G**, the activation energies; Ea (kcal/mol), the reaction energies; Er (kcal/mol) of the hydroboration reaction of the perfect sidewall, BN-doped and NB-doped sidewall of (5,5) armchair single-wall carbon nanotubes (SWNTs).

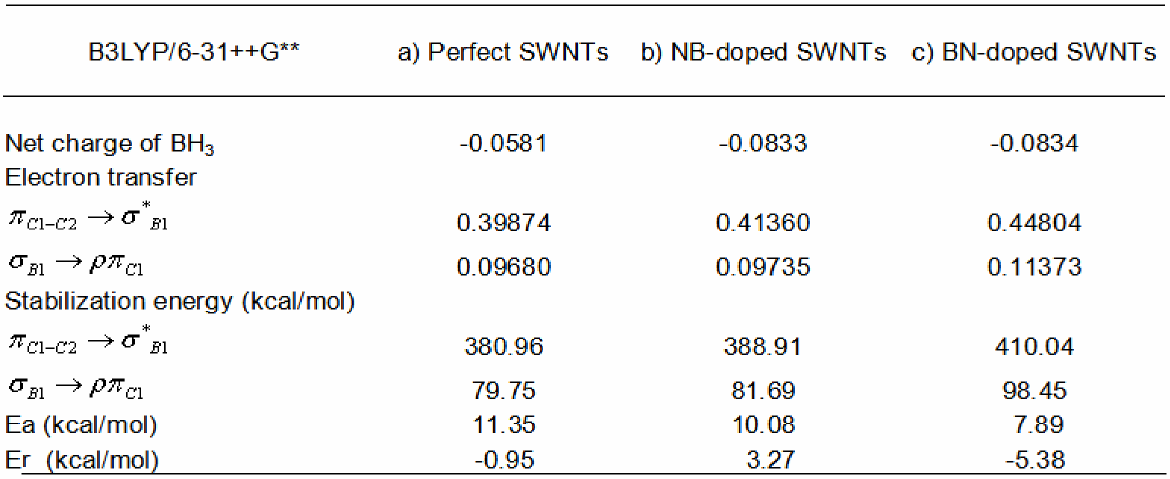

B3LYP/6-31++G**	a) Perfect SWNTs	b) NB-doped SWNTs	c) BN-doped SWNTs
Net charge of BH_3	-0.0581	-0.0833	-0.0834
Electron transfer			
$\pi_{C1-C2} \rightarrow \sigma^*_{B1}$	0.39874	0.41360	0.44804
$\sigma_{B1} \rightarrow p\pi_{C1}$	0.09680	0.09735	0.11373
Stabilization energy (kcal/mol)			
$\pi_{C1-C2} \rightarrow \sigma^*_{B1}$	380.96	388.91	410.04
$\sigma_{B1} \rightarrow p\pi_{C1}$	79.75	81.69	98.45
Ea (kcal/mol)	11.35	10.08	7.89
Er (kcal/mol)	-0.95	3.27	-5.38

[1] Ea = Activation energy of the hydroboration reaction of the sidewalls of SWNTs with borane in kcal/mol.

[2] Er = Reaction energy of the hydroboration reaction of the sidewalls of SWNTs with borane in kcal/mol.

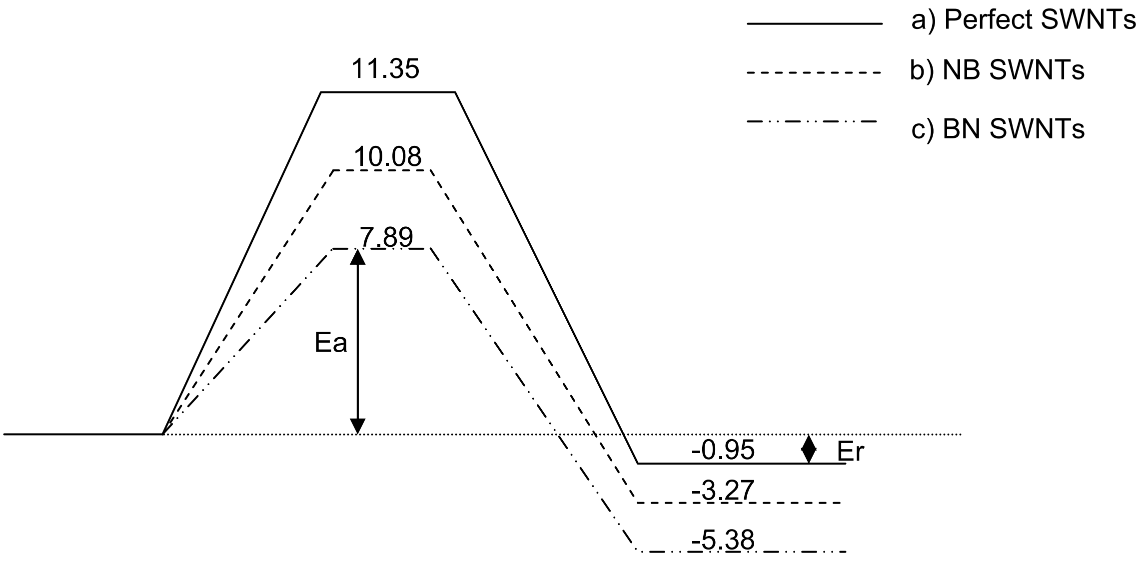

Figure 15 The energy profile of the hydroboration reaction of perfect SWNT, NB doped SWNTs, and BN-doped SWNTs (dash line).

The calculated activation energies (Ea) and the reaction energies (Er) for the hydroboration reaction of the perfect sidewall, NB-doped, and BN-doped with borane are documented in Table 4. The activation barriers of the various three model systems of the sidewall of SWNT considered in this study are 11.35, 10.09 and 7.87 kcal/mol, respectively. It is concluded that the defective structure by boron and nitrogen atoms replaced in the perfect sidewall model is more reactive than that in the perfect sidewall of SWNT due to the reduction of the energy gap in the carbon nanotube Moreover, the charge density at the carbon reactive site plays an important role in enhancing the capability of a Lewis base of nanotubes to donate the electron to the vacant p-orbital of the boron atom in borane via an asynchronous concerted mechanism in the hydroboration reaction.

CONCLUSION

This study has provided the first theoretical demonstration of the effect of B and N substituted C atoms near the carbon reactive center onto 5,5-armchair SWNTs for the hydroboration reaction with borane. Our theoretical study reported the hydroboration reaction of all cases, the perfect sidewall of SWNTs, BN-doped SWNTs, and NB-doped SWNTs could occur via an asynchronous concerted mechanism. The hydroboration reaction of perfect sidewall SWNTs could not prefer to occur easily due to the slight exothermicity. However, the effect of B and N atoms substituted onto the sidewalls of SWNTs could efficiently enhance the reactivity of the hydroboration by increasing kinetic and thermodynamic reactivity. The BN-doped and NB-doped activation energies of the hydroboration which could enhance the reactivity of (5,5) armchair single-wall carbon nanotubes decreased by 4.43 and 3.32 kcal/mol, respectively. The presence of B, N atoms could reduce the energy gap of the tubes, which shift its LUMO and lift the HOMO energy level to enhance the capability of the sidewall of the tube in the hydroboration reaction as shown in Table 3. The BN-doped SWNT is more reactive than NB-doped because of the increasing of the electron density on the π bond on the carbon reactive site which contributes to form a facile four-centered transition state and to stabilize the organoborane product as shown in the higher charge transfer unit.

LITERATURE CITED

Bahr, J. L. and J. M. Tour. 2002. Covalent chemistry of single-wall carbon nanotubes. **J. Mater. Chem.** 12:1952-1958.

_____, J. Yang, D.V. Kosynkin, M.J. Bronikowski, R.E. Smalley and J.M. Tour. 2001. Functionalization of carbon nanotubes by electrochemical reduction of aryl diazonium salts: A bucky paper electrode. **J. Am. Chem. Soc**. 123:6536-6542.

_____ and J.M. Tour. 2001. Highly functionalized carbon nanotubes using in situ generated diazonium compounds. **Chem. Mater.** 13:3823-3*824*.

Becke, A. D. 1993. Density-functional thermochemistry III: The role of exact exchange. **J. Chem. Phys.** 98:5648-5652.

Bethune, D. S., C. H. Kiang, M. D. de Vries, G. Gorman, R. Savoy, J. Vazquez and R. Beyers. 1993. Cobalt-catalysed growth of carbon nanotubes with single-atomic-layer walls. **Nature** 363:605-607.

Bettinger, H. F. 2005. The Reactivity of Defects at the Sidewalls of Single-Walled Carbon Nanotubes: The Stone-Wales Defect. **J. Phys. Chem. B.** 109(15), 6922-6924.

Carroll, D. L., Ph. Redlich, X. Blase, J. C. Charlier, S. Curran, P. M. Ajayan, S. Roth and M. Ruhle. 1998. Effects of nanodomain formation on the electronic structure of doped carbon nanotubes. **Phys. Rev. Lett.** 81: 2332-2335.

Chen, J., M. A. Hammon, H. Hu, Y. S. Chen and A. M. Rao. 1998. Solution properties of single walled carbon nanotubes. **Science** 282:95-98.

Chen, Y., R. C. Haddon, S. Fang, A. M. Rao, P. C. Eklund, W. H. Lee, E. C. Dickey, E. A. Grulke, J. C. Pendergrass, A. Chavan, B. E. Haley and R. E. Smalley. 1998. Chemical attachment of organic functional groups to single-walled carbon nanotube material. **J. Mater. Res.** 13:2423-2431.

Choi, H. J., J. Ihm, S. G. Louie and M. L. Cohen. 2000. Defects, quasibound states, and quantum conductance in metallic carbon nanotubes. **Phys. Rev. Lett.** 84:2917-2920.

Cioslowski, J., N. Rao and D. Moncrieff. 2002. Electronic structures and energetics of [5,5] and [9,0] single-walled carbon nanotubes. **J. Am. Chem. Soc.** 124:8485-8489.

Coleman, S. K., R. S. Bailey, S. Fogden and L. H. M. Green. 2003. Functionalization of single-walled carbon nanotubes via the bingel reaction. **J. Am. Chem. Soc.** 125:8722-8723.

Czerw, R., M. Terrones, J. C. Charlier, X. Blase, B. Foley, R. Kamalakaran, N. Grobert, H. Terrones, P. M. Ajayan, W. Blau, D. Tekleab, M. Ruhle and D. L. Carroll. 2001. Identification of electron donor states in N-doped carbon nanotubes. **Nano Lett.** 1:457-460.

David, Q.N., F. Antonio, G. Carolina, C. Antoni, B. Pablo and M.D. Pere. 2005. Ab initio investigations of lithium insertion in boron and nitrogen-doped single-walled carbon nanotubes . **Chem. Phys. Lett.** 411:256-261.

Dewar, M. J. S., E. G. Zoebisch, E. F. Healy and J. J. P. Stewart, 1984. Development and use of quantum mechanical molecular models AM1: a new general purpose quantum mechanical molecular model. **J. Am. Chem. Soc.** 107:3902-3909.

Ebbesen, T. W. and P. M. Ajayan. 1992. Large-scale synthesis of carbon nanotubes. **Nature** 358:220–222.

Endo, M. 2001. Vapor-grown carbon fibers (VGCFs): Basic properties and their battery applications. **Carbon** 39:1287-1297.

Frisch, M.J., G. W. Trucks, H. B. Schlegel, G. E. Scuseria, M. A. Robb, J. R. Cheeseman, J. A. Montgomery, Jr., T. Vreven, K. N. Kudin, J. C. Burant, J. M. Millam, S. S. Iyengar, J. Tomasi, V. Barone, B. Mennucci, M. Cossi, G. Scalmani, N. Rega, G. A. Petersson, H. Nakatsuji, M. Hada, M. Ehara, K. Toyota, R. Fukuda, J. Hasegawa, M. Ishida, T. Nakajima, Y. Honda, O. Kitao, H. Nakai, M. Klene, X. Li, J. E. Knox, H. P. Hratchian, J. B. Cross, V. Bakken, C. Adamo, J. Jaramillo, R. Gomperts, R. E. Stratmann, O. Yazyev, A. J. Austin, R. Cammi, C. Pomelli, J. W. Ochterski, P. Y. Ayala, K. Morokuma, G. A. Voth, P. Salvador, J. J. Dannenberg, V. G. Zakrzewski, S. Dapprich, A. D. Daniels, M. C. Strain, O. Farkas, D. K. Malick, A. D. Rabuck, K. Raghavachari, J. B. Foresman, J. V. Ortiz, Q. Cui, A. G. Baboul, S. Clifford, J. Cioslowski, B. B. Stefanov, G. Liu, A. Liashenko, P. Piskorz, I. Komaromi, R. L. Martin, D. J. Fox, T. Keith, M. A. Al-Laham, C. Y. Peng, A. Nanayakkara, M. Challacombe, P. M. W. Gill, B. Johnson, W. Chen, M. W. Wong, C. Gonzalez, and J. A. Pople. 2003. **Gaussian 03.** Gaussian, Inc, Pittsburgh, PA.

Georgakilas, V.; K. Kordatos, M. Prato, D.M. Guldi, M. Holzinger and A. Hirsch. 2002. Organic functionalization of carbon nanotubes. **J. Am. Chem. Soc.** 124:760-761.

Haddon, R. C. 1993. Chemistry of the Fullerenes: The Manifestation of Strain in a Class of Continuous Aromatic Molecules. **Science** 261:1545-1550.

_______, G. E. Scuseria and R. E. Smalley. 1997. C240-The most chemically inert fullerene? **Chem. Phys. Lett.** 272:38-42.

Hamon, M. A., M. E. Itkis, S. Niyogi, T. Alvaraez, C. Kuper, M. Menon and R. C. Haddon. 2001. Effect of rehybridization on the electronic structure of single-walled carbon nanotubes. **J. Am. Chem. Soc.** 123:11292-11293.

Hammond, J. S. 1955. A Correlation of Reaction Rates. **J. Am. Chem. Soc.** 77:334-338.

Henderson, C. C. and P.A. Cahill. 1993.C60H2: Synthesis of the Simplest C60 Hydrocarbon dericative. **Science** 259:1885-1887.

Hirsch, A. 2002. Functionalization of single-walled carbon nanotubes. **Angew. Chem., Int. Ed.** 41:1853-1859.

_______, J. Abraham, P. Whelan, R. Graupner, L. Lothar, F. Hennrich, M. Kappes and A. Hirsch. 2003**.** Functionalization of single-walled carbon nanotubes with (R-)oxycarbonyl nitrenes. **J. Am. Chem. Soc**. 125:8566-8580.

Holzinger, M., O. Vostrowsky, A. Hirsch, F. Hennrich, M. Kappes, R. Weiss and F. Jellen. 2001. Sidewall functionalization of carbon nanotubes. **Angew. Chem., Int. Ed.** 40:4002-4005.

Hu, H., B. Zhao, A. M. Hamon, K. Kamaras, E. M. Itkis and C. R. Haddon. 2003. Sidewall functionalization of single-walled carbon nanotubes by addition of dichlorocarbene. **J. Am. Chem. Soc.** 125:14893-14900.

Iijima, S. 1991. Helical microtubules of graphitic carbon. **Nature** 354:56-58.

_______ and T. Ichihashi. 1993. Single-shell carbon nanotubes of 1-nm diameter. **Nature** 363:603-605.

Kroto, H. W., J. R. Heath, S. C. O'Brien, R. F. Curl and R. E. Smalley. 1985. C_{60}: Buckminsterfullerene. **Nature** 318:162-163.

Lee, C., W. Yang and R. G. Parr. 1988. Development of the Colle-Salvetti correlation-energy formula into a functional of the electron density**.** **Phys. Rev. B** 37:785-789.

Lu, X., F. Tian, N. Wang and Q. Zhang. 2002. Organic functionalization of the sidewalls of carbon nanotubes by diels-alder reactions: a theoretical prediction. **Org. Lett.** 24:4313-4315.

_______, L. Zhang, X. Xu, N. Wang and Q. Zhang 2003. Can the sidewalls of single-wall carbon nanotubes be ozonized? **J. Phys. Chem. B** 106:2136-2139.

_______, F. Tian, X. Xu, N. Wang and Q. Zhang. 2003. A theoretical exploration of the 1,3-dipolar cycloadditions onto the sidewalls of [n,n] armchair single-walled carbon nanotubes. **J. Am. Chem. Soc.** 125:10459-10464.

Malcioglu, O. B., E. Tasci and S. Erkoc. 2005. Structural and molecular electronic properties of BN ring doped single-wall carbon naotubes. **Physica E** 28(3): 296-308.

Martin, N., M. Altable, S. Filippone, A. M. Domenech, L. Echegoyen and C. M. Cardona. 2006. Retro-cycloaddition reaction of pyrrolidinofullerenes. **Angew. Chem. Int. Ed.** 45:110-114.

Matsuo, Y., K. Tahara and E. Nakamura. 2003. Theoretical studies on structures and aromaticity of finite-length armchair carbon nanotubes. **Org. Lett.** 5:3181-3184.

Mawhinney, D. B., V. Naumenko, A. Kuznetsova, J. T. Yates, J. Liu and R. E. Smalley. 2000. Infrared spectral evidence for the etching of carbon nanotubes: ozone oxidation at 298 k. **J. Am. Chem. Soc.** 122:2383-2384.

McKee, M. L. and C. M. Rohlfing. 1981. An ab initio study of complexes between ethylene and ozone. **J. Am. Chem. Soc.** 111:2497-2500.

Mickelson, E. T., C. B. Huffman, A. G. Rinzler, R. E. Smalley, R. H. Hauge and J. L. Margrave.1998. Fluorination of single-wall carbon nanotubes. **Chem. Phys. Lett.** 296:188-194.

Mintmire, J. W., B. I. Dunlap and C. T. White. 1992. Are fullerene tubules metallic? **Phys. Rev. Lett.** 68:631-634.

Namuangruk, S., P. Pantu and J. Limtrakul. 2004. Alkylation of benzene with ethylene over faujasite zeolite investigated by the ONIOM method. **J. Catal**. 225:523-530.

_______, P. Pantu and J. Limtrakul. 2005. Investigation of ethylenedimerization over faujasite zeolite by the ONIOM method**. ChemPhysChem** 6:1333-1339.

Neeb, P., O. Horie and K.G. Moortgat.1998. The ethene-ozone reaction in the gas phase. **J. Phys. Chem. A** 102:6778-6785.

Niyoki, S., M. A. Hamon, H. Hu, B. Zhao, P. Bhowmik, R. Sen, M. E. Itkis and R.C. Haddon. 2002. Chemistry of single-walled carbon nanotubes. **Acc. Chem. Res.** 35:1105-1113.

Odom, T. W., J. L. Huang, P. Kim, M. Ouyang and C. M. Lieber. 1998. Scanning tunneling microscopy and spectroscopy studies of single-walled carbon nanotubes. **J. Mater. Res.** 13:2380-2388.

_______, J. L. Huang, P. Kim and C. M. Lieber. 1998. Atomic structure and electronic properties of single-walled carbon nanotubes. **Nature** 391:62-64.

Pekker, S., J.-P. Salvetat, E. Jakab, J.-M. Bonard and L. Forró. 2001. Hydrogenation of carbon nanotubes and graphite in liquid ammonia. **J. Phys. Chem. B** 105:7938-7943.

Peng, C. and H.-B. Schlegel, 1994. Combining synchronous transit and quasi-Newton methods to find transition states. **Isr. J. Chem**. 33: 449-454.

Peng, C., P.Y. Ayala, H.B. Schlegel and M.J. Frisch. 1996. Using redundant internal coordinates to optimize equilibrium geometries and transition states. **J. Comput. Chem**. 17:49-56

Saito, R., R. Saito, M. Fujita, G. Dresselhaus and M. S. Dresselhaus. 1992. Electronic-structure of chiral graphene tubules. **Appl. Phys. Lett.** 60:2204-2206.

Schleyer, P. V. R., C. Maerker, A. Dransfeld, H. Jiao and N. E. Hommes. 1996. Nucleus-Independent Chemical Shifts: A Simple and Efficient Aromaticity Probe. **J. Am. Chem. Soc.** 118:6317-6318.

Sondheimer, F., Y. Gaoni, L. M. Jackman, N. A. Bailey and R. Mason. 1996. 1,8-Bisdehydro [4] Annulene, an Unusual Aromatic Compound. **J. Am. Chem. Soc.** 84:4595-4596.

Stanislaus S. W., E. Joselevich, A. T. Woolley, C. L. Cheung and C. M. Lieber. 1998. Covalently functionalized nanotubes as nanometre-sized probes in chemistry and biology. **Nature** 394:52–55.

Star, A., J. Stoddart, D. Steuerman, M. Diehl and A. Boukai. 2001. Preparation and properties of polymer-wrapped single-walled carbon nanotubes. **Angew. Chem., Int. Ed.** 40:1721-1725.

Sun, Y., K. Fu, Y. Lin and W. Huang. 2002. Functionalized carbon nanotubes:properties and applications. **Acc. Chem. Res.** 35:1096-1104.

_____, S.R. Wilson and D.I. Schuster, 2001. High dissolution and strong light emission of carbon nanotubes in aromatic amine solvents. **J. Am. Chem. Soc.** 123:5348-5349.

Taylor, R. and D. M. R Walton. 1993. The Chemistry of the Fullerenes. **Nature** 363:685-687.

Tang, S. C., P.J.F. Harris and M.L.H. Green. 1993. Thinning and opening of carbon nanotubes by oxidation using carbon dioxide. **Nature** 362:520-522.

Terrones, M., A. Jorio, M. Endo, A.M. Rao, Y.A. Kim, T. Hayashi, H. Terrones, J.-C. Charlier, G. Dresselhaus and M.S. Dresselhaus. 2004. Block copolymer patterns and templates. **Materials Today** 7(10):30-39.

Venerma, L.C., Meunier, V. Lambin, P. Dekker and C. Datum. 2000. Atomic structure of carbon nanotubes from scanning tunneling microscopy. **Phys. Rev. B** 61:2991-2996.

Warakulwit, C., S. Bamrungsap, P. Luksirikul, P. Khongpracha and J. Limtrakul. 2005. Diels-Alder cycloadditions of single-wall carbon nanotubes with electron-rich dienes: a theoretical study. **Stud. Surf. Sci. Catal.** 156:823-828.

Wildoer, J. W. G., L. C. Venema, A. G. Rinzler, R. E. Smalley and C. Dekker. 1998. Electronic structure of atomically resolved carbon nanotubes. **Nature** 391:59-62.

Yamashita, J., H. Hirayama, Y. Ohshima and K. Takayanagi. 1999. Growth of a single-wall carbon nanotube in the gap of scanning tunneling microscope. **Appl. Phys. Lett.** 74:2450-2452.

Ying, Y., R. K. Saini, F. Liang, A. K. Sadana and W. E. Billups. 2003. Functionalization of carbon nanotubes by free radicals. **Org. Lett.** 5:1471-1473.

Yumura, T., K. Hirahara, S. Bandow, K. Yoshizawa and S. Iijima. 2004. A theoretical study on the geometrical features of finite-length carbon nanotubes capped with fullerene hemisphere. **Chem. Phys. Lett.** 386:38–43.

Zhang, C., R. Li, D. Zhang, Z. Shang, G. Wang, Y. Liang, Y. Xing, Y. Pan, Z. Cai, X. Zhao and C. Liu. 2006. Theoretical explorations on BN-doped armchair single-walled carbon nanotubes**. J. Mol. Struc. (THEOCHEM)** 765:1-11.

Zhou, Z., X. Gao, J.Yan and D. Song. 2006. Doping effects of B and N on hydrogen adsorption in single-walled carbon nanotubes through density functional calculations. **Carbon** 44(5): 939-947.